

Inverse Bicontinuous Cubic Phases in 2:1 Fatty Acid/Phosphatidylcholine Mixtures. The Effects of Chain Length, Hydration, and Temperature

R. H. Templer,* J. M. Seddon, N. A. Warrender, A. Syrykh, and Z. Huang

Department of Chemistry, Imperial College, London SW7 2AY

R. Winter and J. Erbes

University of Dortmund, Institute of Physical Chemistry I, D-44221 Dortmund

Received: August 29, 1997; In Final Form: June 23, 1998

Using small-angle X-ray diffraction and polarizing microscopy, we have investigated the phase and structural behavior of inverse bicontinuous cubic phases in a homologous series of 2:1 (mol:mol) saturated fatty acid/phosphatidylcholine mixtures in water. For the C₁₂ fatty acid/phosphatidylcholine mixtures, we find three inverse bicontinuous cubic phases, which our analyses indicate are based upon the P, D, and G minimal surfaces. Between 35 and 49 °C these phases are observed to occur in the sequence G → D → P as the water content is increased. The excess water P cubic disappears above 49 °C when it is replaced by the D cubic in coexistence with the inverse hexagonal phase. For C₁₄ fatty acid/phosphatidylcholine mixtures, we find only the P cubic in coexistence with the inverse hexagonal phase. For longer chain length fatty acid/phosphatidylcholine mixtures, the inverse bicontinuous cubics are entirely absent, their place being taken by the inverse hexagonal phase. Most of our evidence for the structure of the cubic phases being based on the P, D, and G minimal surfaces comes from our modeling of the isothermal swelling data in the C₁₂ system. This modeling has also been used to fit the swelling behavior in the inverse hexagonal phase and has allowed us to determine the location of the pivotal surface for the 2:1 fatty acid/phosphatidylcholine mixtures for chain lengths between C₁₂ and C₁₈. With little variation as a function of chain length or hydration, the pivotal surface appears to be located between the second and third CH₂ groups of the hydrocarbon chains with an average molecular area per 2:1 (mol:mol) saturated fatty acid/phosphatidylcholine complex of 109.5 ± 1.5 Å². As far as we are aware this is the first self-consistent determination of pivotal surface geometry spanning four phases and four different chain lengths.

1. Introduction

In this paper we report on the appearance of liquid crystalline inverse bicontinuous cubic phases in the phase diagrams of a homologous series of saturated 2:1 (mol:mol) fatty acid/phosphatidylcholine mixtures in water (henceforth 2:1 FA/PC). We have used small-angle X-ray diffraction to measure structural changes in these phases as a function of water composition and temperature and then attempted to fit the swelling behavior using geometrical models of the inverse bicontinuous cubic phases and the inverse hexagonal phase. Not only does this modeling provide us with strong evidence for the nature of the structure of the cubic phases, but it also allows one to determine the molecular location about which the monolayer bends: the pivotal surface. The location of the pivotal surface is central to modeling the energetics of interfacial bending in these phases, and in a companion paper we have used these measurements to determine the energetic conditions which favor the inverse bicontinuous cubic phases over the inverse hexagonal phase.¹

The study and interpretation of the inverse bicontinuous cubic phases is less esoteric than might at first appear. Their presence in a wide range of biological membrane structures has recently been demonstrated.² Furthermore there is mounting evidence that the structural forces which give rise to these lyotropic phases are important in enzyme regulation³ and that the formation of structure elements with the same topology as the bicontinuous cubics are involved in membrane fusion.⁴ In relation to these

latter effects it is well-known that fatty acids affect membrane permeability⁵ and fusion.⁶ More recently, they have also been shown to regulate the activity of specific ion channels.⁷ Although the levels of fatty acids present in biological membranes are significantly lower than those used in our study, the structural forces in the membrane which promote the inverse bicontinuous cubic phases will also be at play in the biological systems. For example, the stresses that a fatty acid molecule sets up in the bilayer may well exert important functional control on bilayer spanning proteins.⁸

The most commonly found inverse bicontinuous cubic phases in lipid/water mixtures are the structures shown in Figure 1. These consist of a single lipid bilayer which partitions all space into two, congruent, aqueous, subvolumes. We will refer to the three cubics as Q_{II}^P, Q_{II}^D, and Q_{II}^G, where the subscript indicates a type II, or inverse mesophase and the superscript refers to the mathematicians' nomenclature for the periodic minimal surfaces which these structures are believed to be based upon.⁹ The minimal surface lies at the bilayer midplane, that is at the average location of the terminal methyl groups of the amphiphiles. The minimal surface has the property that the mean curvature defined as half the sum of the principal curvatures c_1 and c_2 is zero everywhere on the surface. This occurs because $c_1 = -c_2$ everywhere. However, when we drape a bilayer over the minimal surface, the polar/apolar interface on either side of the minimal surface will always have a net

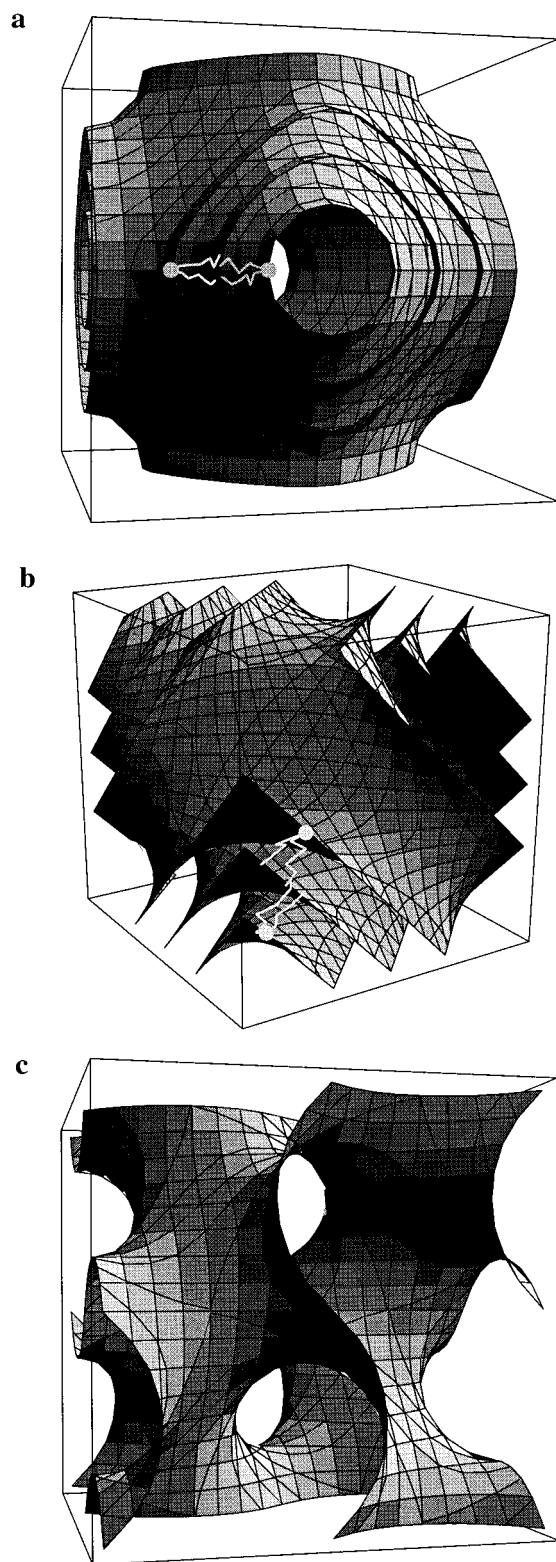


Figure 1. The inverse bicontinuous cubic phases. The unit cells of (a) the P cubic, space group $Im3m$, symbol Q_{II}^P , (b) the D cubic, space group $Pn3m$, symbol Q_{II}^D , and (c) the G cubic, space group $Ia3d$, symbol Q_{II}^G , are illustrated. In a and b the location of the amphiphiles is shown. For reasons of clarity we have only shown the bilayer midplane (the underlying periodic minimal surface) for Q_{II}^G .

mean curvature toward the water.¹⁰ By convention we make the sign of the mean curvature in such cases negative.

The inverse bicontinuous cubic phases are therefore just one topological solution to the system's need to find a mesophase

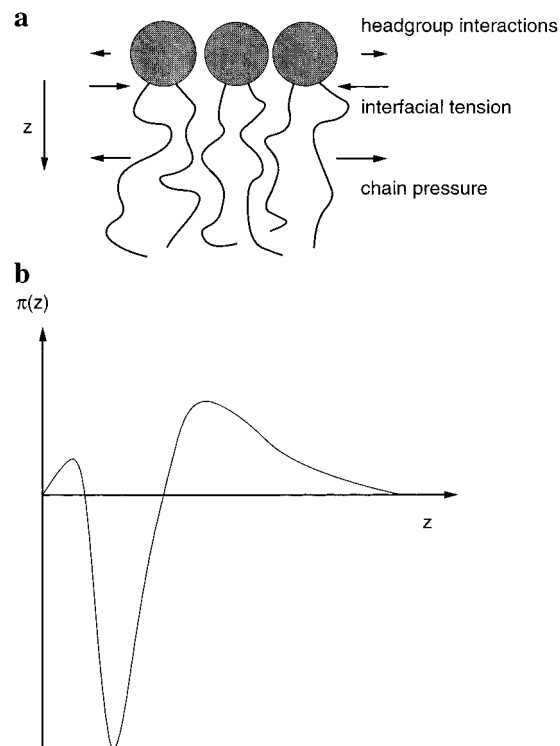


Figure 2. The differential lateral pressure profile and its molecular origins. Distinct local intermolecular forces are at play as a function of depth, z , through the monolayer a. Such interactions will give rise to a lateral pressure profile having the qualitative form shown in b.

structure in which the polar/apolar interface can bend toward the aqueous component. The desire for negative mean interfacial curvature arises because of the differential lateral pressures which are present across the monolayer film.

The lateral pressure in a flat monolayer varies in the way shown in Figure 2. In the chain region the pressure must be a positive outward one, if the chains are molten. Theoretical calculations tell us that the chain lateral pressure varies as we approach the interface, generally reaching a maximum around the first few CH_2 groups.¹¹ Around the interface the pressure is negative because of the interfacial tension between the hydrocarbon rich and water rich regions of the monolayer. Around the headgroup region we might expect to sense positive pressure once again, due to steric and hydrational repulsion between headgroups. However, in some cases it is believed that the pressure may be negative due to direct hydrogen bonding between headgroups, indeed it is suspected that there are hydrogen bonded complexes between phosphatidylcholine and fatty acid molecules.¹² In a case where there is weak repulsion (or possibly even attraction) between headgroups and strong outward pressure in the chain region, it is clear that the interface will wish to bend toward the water.

The general effect of adding saturated fatty acids to the same chain length saturated phosphatidylcholine is already quite well-known, particularly under conditions where the lipids are fully hydrated.^{13,14} In particular it has been observed that at mole ratios of one phosphatidylcholine to two fatty acids and with chain lengths greater than C_{14} , the mixtures undergo a chain melting transition from the L_β gel phase directly to the inverse hexagonal or H_{II} phase, Figure 3. In other words they are exhibiting a distinct desire for negative mean curvature. This is in sharp contrast to the normal chain melting transition for phosphatidylcholine molecules on their own, which is to the fluid lamellar or L_α phase.¹⁵ Indeed, this is the ubiquitous liquid

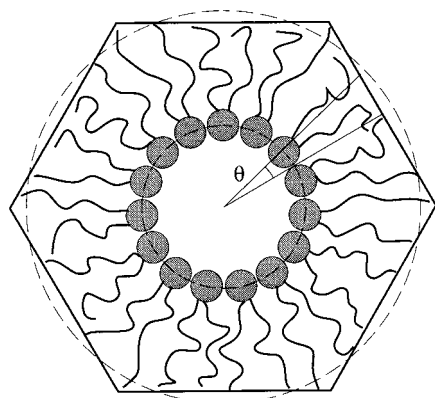


Figure 3. A perpendicular cross section of the inverse hexagonal phase. Chains must extend into the corners of the unit cell and compress against the flat faces.

crystalline phase in phosphatidylcholines, which leads one to suppose that the addition of the two fatty acid molecules has made a significant difference to the structural forces which destabilize the flat lamellar phase and give rise to phases with interfacial curvature.

If the system does undergo a phase transition to one in which there is monolayer curvature, the choice is topologically limited to interfaces which are either elliptic, cylindrical, or saddle shaped. For the inverse mesophases the only properly identified case of an elliptic interface is the *Fd3m* micellar cubic, which we will not discuss here.¹⁶ Cylindrical interfaces pack on a two-dimensional hexagonal lattice in the H_{II} phase, Figure 3, and the saddle shaped interfaces are of course found in the inverse bicontinuous cubics of Figure 1. In all cases such interfacial geometries exhibit negative mean curvature and hence reduced molecular cross sectional areas at the interface.

However, it is impossible to achieve both uniform mean interfacial curvature and pack the hydrocarbon region with uniform chainlength.^{17,18} This is most easily observed in the H_{II} phase, Figure 3. If we insist that the interface be a cylinder of uniform radius, in an attempt to give each molecule the same amount of splay, then there must be a variation in the monolayer thickness, with hydrocarbon chains being stretched into the hexagonal corners of the unit cell and somewhat compressed along the hexagonal faces. If conversely we insist that the monolayer have uniform thickness, then the system must suffer variations in mean interfacial curvature, with most of the interface being flat and the regions near the hexagonal corners having highly negative mean curvature. Such physical frustration arises in all of the mesophases, including the bicontinuous cubics. Naturally the system will seek a compromise between these extremes of constant monolayer thickness and constant mean curvature.

It is in modeling this competition between the desire for uniform curvature and the need to pack the monolayer space uniformly that it is thought that we may understand the processes which both drive and stabilize the observed mesophase behavior.^{17,18}

An important consequence of such modeling is that we discover some simple relationships between the geometry of the bicontinuous cubic phases in excess water, which we have previously reported.¹⁹ We will use these results as an element in confirming the presence of the bicontinuous structures. The rest of the evidence comes from modeling measurements of the effects of water content on the geometry of the inverse bicontinuous cubic phases. Our modeling of the swelling behavior of the inverse mesophases assumes that there is a part

of the molecules which does not alter in cross-sectional area during isothermal bending. This is termed the pivotal surface.^{20,21} The molecular dimensions of the pivotal surface have been determined for our homologous series of 2:1 FA/PC mixtures. The data that we have collected on phase stability as a function of water content, temperature, and chain length is also reported. We discuss some apparently universal aspects of the phase behavior in terms of the ideas discussed above.

2. Materials and Methods

The phospholipids 1,2-dilauroyl-*sn*-glycero-3-phosphocholine (DLPC), 1,2-dimyristoyl-*sn*-glycero-3-phosphocholine (DMPC), 1,2-dipalmitoyl-*sn*-glycero-3-phosphocholine (DPPC), and 1,2-distearoyl-*sn*-glycero-3-phosphocholine (DSPC) were purchased from Avanti Polar Lipids, Inc. (Birmingham, AL) and Larodan Fine Chemicals AB (Malmo, Sweden). Lauric acid (LA), myristic acid (MA), palmitic acid (PA), and stearic acid (SA) were purchased from the Aldrich Chemical Co. (Gillingham, UK). All commercial materials used were of the highest purity available (>99%) and were subsequently used without further purification.

Stock 2:1 FA/PC mixtures were prepared by codissolving phosphatidylcholine and fatty acid in a mixture of cyclohexane and chloroform (approximately 3:1 by volume). To calculate the appropriate amounts of each component to give a 2:1 molar ratio, we always assumed that the phosphatidylcholine was the dihydrate. Once mixed the solution was then gently evaporated under a stream of dry nitrogen, until it achieved the consistency of treacle before being lyophilized at liquid nitrogen temperature. A weighed amount of the resulting dry white powder was simply dropped into 1.5 mm diameter, thin walled X-ray capillaries under a dry nitrogen atmosphere and a weighed amount of fresh, deionized, triply distilled water added. The sample mass was typically between 5 and 10 mg and our calculations of sample hydration assumed that, once freeze-dried in the presence of the fatty acid, the phosphatidylcholine was anhydrous. The X-ray capillaries were flame sealed and the samples were mixed by centrifuging the sample up and down the capillary after incubation above the chain melting transition. It was difficult to ensure that low water content samples which were in a bicontinuous cubic phase were uniformly hydrated. We guarded against this by measuring the lattice parameter at various points in the X-ray capillary. Only samples where fluctuations in the lattice parameter were within $\pm 2\%$ have been reported here.

As far as we were able to determine, 2:1 FA/PC samples made in this way were perfectly mixed. We did not observe any bulk phase separation in X-ray diffraction from the liquid crystalline mesophases. In other words, for the data we report here we saw no evidence of independent lamellar peaks which could be ascribed to phase separated fatty acid.

X-ray diffraction measurements were made on a GX-20 rotating anode generator (Enraf-Nonius, Netherlands) using a 100 μm focus cup run at 750 W. A Franks double mirror camera with 200 mm focal length was used to focus the beam to a spot 160 μm in height and 110 μm in width (measured as the full width at half-maximum). Partial monochromatization was achieved with a nickel filter selecting the Cu $K\alpha$ lines ($\lambda = 1.54 \text{ \AA}$). A set of adjustable tungsten slits approximately 15 mm before the sample reduced parasitic scattering to levels where we were able to measure lattice spacings up to 400 \AA . The capillaries were placed in a copper sample holder with thermoelectric temperature control between -30 and 80°C . Temperature control was measured to be within $\pm 0.03^\circ\text{C}$. The optics and the sample cell were both held under vacuum to

minimize air scatter. The sample cell chamber included a variable length, evacuated flight path, allowing the X-ray detector to be placed between 120 and 300 mm from the sample, thereby taking advantage of the long focal depth of the Frank optics. The design of our sample chamber limited wide angle measurements to a minimum spacing of 3.5 Å.

The X-ray diffraction was recorded on an image intensified CCD based two-dimensional detector adapted from a previously reported design.^{22,23} The entire X-ray system was placed under computer control, allowing us to automate the acquisition and analysis of data. The parsed program environment used for this is called TV4, designed by S. M. Gruner of Princeton University and E. F. Eikenberry of Rutgers University. The program has been tailored to operate our detector and communicate with the off-board control system we use to operate our thermoelectric heaters.

In our X-ray diffraction measurements we made temperature steps of 2.5 °C and then allowed the sample to equilibrate for at least 10 min before acquiring the X-ray pattern. Repeated runs on a single sample, using this protocol, gave results which were reproducible to ± 1.5 Å in the lattice parameter. Phase transition temperatures measured on a single sample, using this protocol were reproduced to ± 1 °C. Extending the equilibration time from 10 to 30 min did not alter the measurement of lattice parameter or phase transition temperature. However, the variations we found from one sample preparation to another were greater than those reported above. The measured variation (to 1 standard deviation) in the cubic lattice parameters decreased from ± 4 Å for the largest cubics with lattice parameters up to 180 Å down to ± 1.5 Å for lattice parameters below 100 Å. It is these errors which are quoted in the graphs of our data. For the H_{II} phase the uncertainty is estimated to be ± 0.6 Å. Variations in transition temperature measurements are presented in some detail in section 3.1.

X-ray structural measurements require the determination of sample density. These measurements were made 10 °C above the chain melting temperature using a DMA 602/60 oscillating U-tube density meter (Anton Paar, K. G., Graz, Austria). The water volume fraction, ϕ_w , of our sample could then be determined via

$$\phi_w = \left(1 + \frac{\rho_w m_l}{\rho_l m_w} \right)^{-1} \quad (1)$$

where ρ_w and ρ_l are the densities of water and the 2:1 FA/PC mixtures, respectively, and m_w and m_l are the respective masses of the lipid mixture and water. It should be noted that in our calculations we treat the two fatty acids and one phosphatidylcholine molecule as if they were a single lipid amphiphile (i.e., ρ_l is the density of the lipid mixture). Therefore the values for molecular volumes and cross-sectional areas we present in this paper refer to a 2:1 FA/PC complex. The error in the calculation of water volume fraction is largely due to the uncertainties in the measurement of component masses. We can measure component masses with a precision of 1 μ g, but the measurements are only reproducible to ± 5 μ g. We use this uncertainty to calculate errors in ϕ_w .

In addition to X-ray measurements, we made phase identifications by polarizing microscopy, using a Nikon Labophot microscope (Nikon Ltd., Telford, UK). Water penetration samples for this work were prepared by melting dry sample on a glass slide and then placing one edge of a square coverslip over the resulting droplet. Two coverslips were placed under the opposite edge of the first one to form a shallow ramp. The

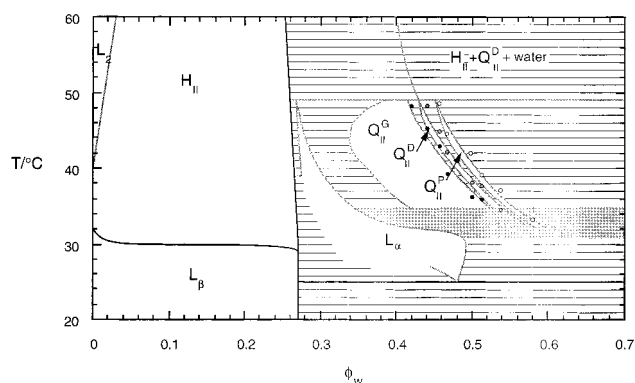


Figure 4. The temperature/water composition phase diagram for 2:1 LA/DLPC at atmospheric pressure. Those phase boundaries which are the least well characterized are shown in gray. Data points used to locate the phase boundaries between the cubic phases are shown ($Q_{II}^G \rightarrow Q_{II}^D$, black circles, $Q_{II}^D \rightarrow Q_{II}^P$, gray circles, and $Q_{II}^P \rightarrow$ excess water, white circles). Their scatter gives some impression of the precision with which we were able to locate the less well characterized phase boundaries.

sample was then cooled and water introduced into contact with the edges of the wedge of sample. The temperature controller (TH600, Linkam Scientific Instruments, Tadworth, UK) was slowly ramped up in temperature (less than 1 °C min⁻¹), and photographs were taken of the phases which formed.

3. Results and Structural Analysis

We begin, section 3.1, by examining the phase behavior of the 2:1 FA/PC mixtures as a function of water composition and temperature. We then model our data on the swelling of the inverse hexagonal and bicontinuous cubic phases in section 3.2.

3.1. Phase Behavior of 2:1 FA/PC Mixtures. The phase diagram for 2:1 LA/DLPC as a function of water volume fraction and temperature is shown in Figure 4. The phase diagram has been constructed both from X-ray structural studies at fixed water contents ($\phi_w = 0.000, 0.094, 0.153, 0.174, 0.205, 0.235, 0.258, 0.266, 0.283, 0.376, 0.389, 0.396, 0.420, 0.4475, 0.458, 0.473, 0.500, 0.508, 0.539, 0.579$, and excess) and water penetration studies using polarizing microscopy and represents the system's behavior upon heating. Where our determination of phase boundaries are reasonably accurate (± 1 °C and ± 0.005 in ϕ_w), the boundaries have been drawn in black. The boundaries drawn in gray are less accurately determined. Their relative ordering with respect to the water composition is correct, but the absolute location of the water volume fraction at which phase boundaries occur are accurate to no more than ± 0.01 . To give some impression of the agreement between the phase boundaries and our data, we have superimposed the experimental points used to locate the boundaries between the three cubic phases.

Although it is not central to the purpose of this paper, we have included our data on the phase behavior below 30 °C. Below the chain melting transition at 30 °C the system is predominantly in an L_β phase. However, at water volume fractions in excess of approximately 0.27 we have visual and X-ray evidence of an L_α phase down to a temperature of approximately 25 °C.

Above 30 °C polarizing microscopy shows that the L_α phase is bounded at lower water contents by an H_{II} phase. As we increase temperature, the lamellar phase imbibes water (up to $\phi_w \approx 0.48$) before we observe the next phase transition around 32 °C into the three inverse bicontinuous cubic phases Q_{II}^P , Q_{II}^D , and Q_{II}^G .

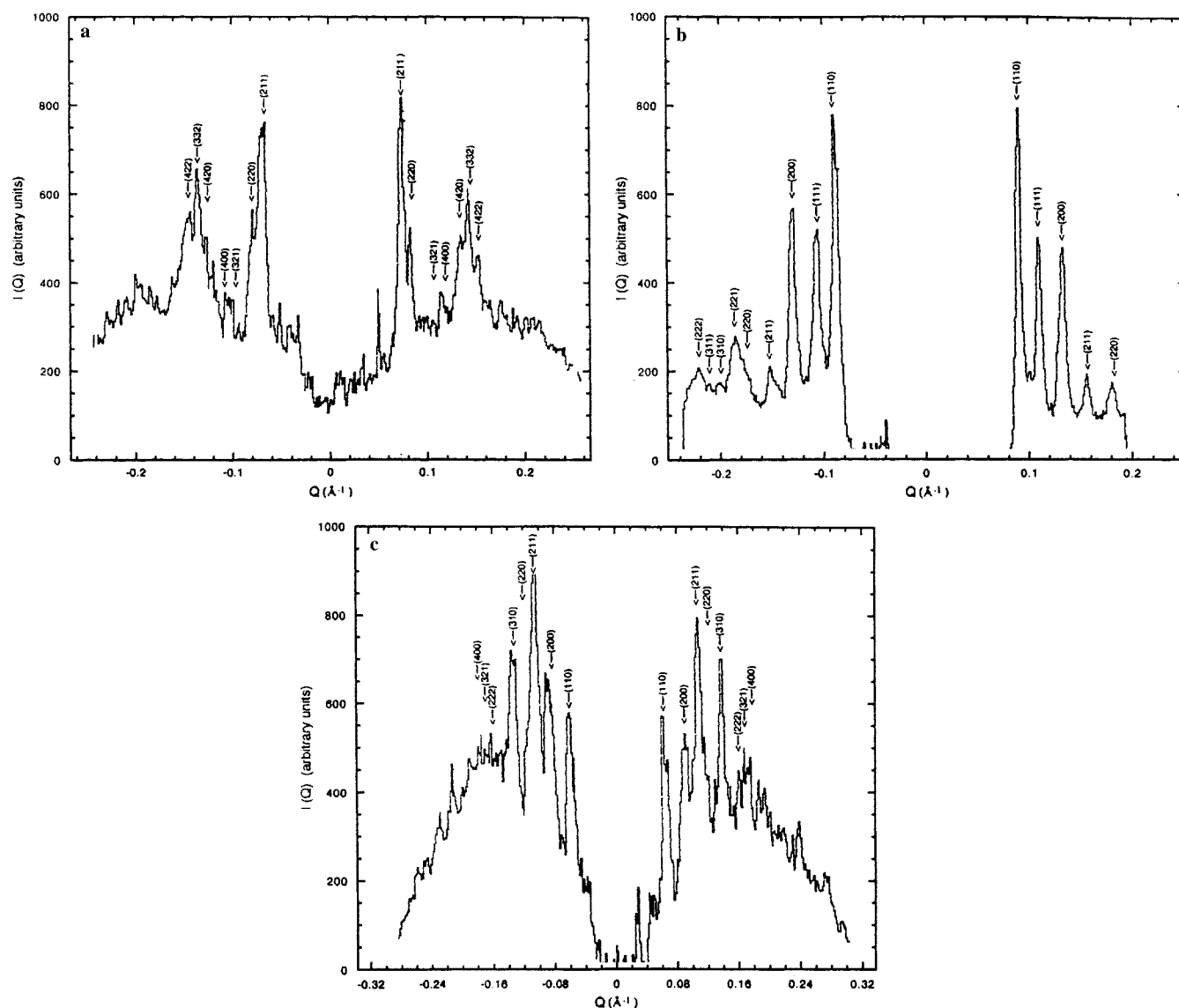


Figure 5. Typical X-ray diffraction profiles for (a) Q_{II}^G , (b) Q_{II}^D , and (c) Q_{II}^P . In a the $\sqrt{6}$, $\sqrt{8}$, $\sqrt{20}$, $\sqrt{22}$, and $\sqrt{24}$ reflections are clearly visible above the detector noise, but the $\sqrt{14}$ and $\sqrt{16}$ reflections are barely visible. In b the diffraction is particularly strong, and we observe diffraction up to the ninth order, although some of the higher order peaks are rather dim. In c the diffraction is weaker and only the $\sqrt{2}$, $\sqrt{4}$, $\sqrt{6}$, and $\sqrt{10}$ are clearly visible above detector noise. The $\sqrt{8}$ peak is typically absent, but the other orders indicated are often seen.

Of the cubic phases Q_{II}^G (space group $Ia3d$) appears at the lowest water volume fractions. Polarizing microscopy clearly shows that this phase is next to the L_α phase at low temperatures and hydrations. Generally we are able to detect the reflections for the $Ia3d$ cubic between (211) and (422), although (321) and (400) are weak, Figure 5a. The Q_{II}^D phase (space group $Pn3m$) appears over a fairly narrow range of water content, sandwiched between Q_{II}^G and Q_{II}^P . When present, the phase is quite straightforward to identify. We are often able to record at least the first 6 reflections (110), (111), (200), (211), (220), and (221) which characteristically exhibit a monotonic decrease in the intensity of the reflections with increasing order, Figure 5b. Q_{II}^P (space group $Im3m$) is also quite straightforward to identify. We are always able to detect the first three orders (110), (200), (211), which have a characteristic intensity distribution, Figure 5c. With longer exposures we are able to resolve as far out as the tenth order reflection and always observe that the (220) reflection is too weak to be observed. This latter observation is consistent with the structure factor calculations for Q_{II}^P .²⁴ The Q_{II}^P phase projects out to a water volume fraction of 0.60

± 0.03 at 32 °C. At this point it has a lattice parameter of 180 ± 4 Å. The presence of the three cubic phases is clearly visible under the polarizing microscope.

The transition region between the L_α phase and the inverse bicontinuous cubic phases appears to be quite complex. Certainly, polarizing microscopy indicates coexistence in the transition region between the lamellar and cubic phases. Our X-ray data indicates that the transition may also involve intermediate, metastable states, with lifetimes of the order of several minutes. It may be possible that these are a mixture of lamellar, hexagonal, and cubic phases, but the appearance of these signals is so unpredictable that we have yet to elucidate the nature of the transitions. As a consequence we have left this region of the phase diagram gray to indicate our lack of precise phase information.

As temperature is increased the cubic phase boundaries move to lower hydration quite rapidly and the H_{II} phase boundary less so. This can be seen directly from the X-ray diffraction measurements of lattice parameter as a function of temperature in excess water, Figure 6. The reader should in particular note

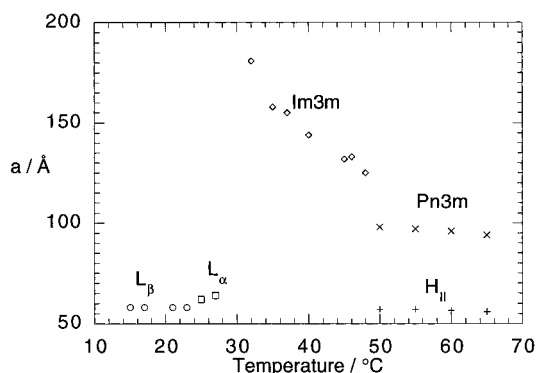


Figure 6. The temperature dependence of the lattice parameters a of the excess water phases in 2:1 LA/DLPC. The lattice parameter of the H_{II} phase is defined to be the distance between the nearest neighbor water cylinders.

the fact that the change in lattice parameter as a function of temperature is greatest for Q_{II}^P (ca. 3.5 Å/°C), least for H_{II} (ca. 0.05 Å/°C), Q_{II}^D and intermediate for Q_{II}^G (ca. 0.2 Å/°C).

As we raise the temperature above 49 °C , we destabilize Q_{II}^P in favor of coexisting H_{II} and Q_{II}^D phases. In fact the transition boundary, measured in excess water is variable in our experiments, ranging between 49 and 58 °C , depending on the sample set, although within a single sample set the transition temperature is reproducible to within 2° , and where there is little excess water the variation in the boundary's location reduces considerably to between 49 and 53 °C . From our microscopy work it appears that the H_{II} phase appears in coexistence with Q_{II}^D at the same temperature as both the lamellar, Q_{II}^D , and Q_{II}^P phases disappear. The coexisting H_{II} phase appears very suddenly as rather small, birefringent, granular inclusions within the viscous isotropic matrix of the cubic phases. The H_{II} phase is clearly seen by X-ray diffraction, and as far as we are able to determine, no bicontinuous cubic phases other than Q_{II}^D are to be found in coexistence with it above the phase transition temperature shown at 49 °C . This is in agreement with our observations from the optical penetration scan.

All we have done so far is to identify the space group of each of the cubic phases. Our first evidence that these are indeed the bicontinuous cubics shown in Figure 1 is the relationship between the equilibrium lattice parameters, Q_{II}^P and Q_{II}^D of the P and D cubic, respectively. For example, in excess water we find that at the phase transition boundary between Q_{II}^P and Q_{II}^D at 49 °C , $a_P/a_D = 1.28 \pm 0.02$, which is in agreement with the theoretically predicted value of 1.279 .¹⁹ The fact that we find the ratio a_P/a_D to be in agreement with theory leads us to the identification of these phases with bicontinuous cubics based on the P and D minimal surfaces. Further compelling evidence for this identification and for Q_{II}^G being based on the G minimal surface is to be found in section 3.2.

The phase diagram for 2:1 MA/DMPC, Figure 7, was determined from X-ray diffraction data on samples of fixed water composition ($\phi_w = 0.000, 0.055, 0.079, 0.098, 0.124, 0.190, 0.223, 0.274, 0.277, 0.344, 0.380, 0.386, 0.458, 0.532$, and excess). The most dramatic difference in this phase diagram is that although we do observe at least one of the bicontinuous cubic phases, Q_{II}^P , it is always found in coexistence with the H_{II} phase. In excess water we have been able to detect Q_{II}^P between the chain melting transition and approximately 70 °C , beyond which temperature we only observe the H_{II} phase.

At water contents intermediate between the excess point for H_{II} and the composition of Q_{II}^P , we have some rather ambigu-

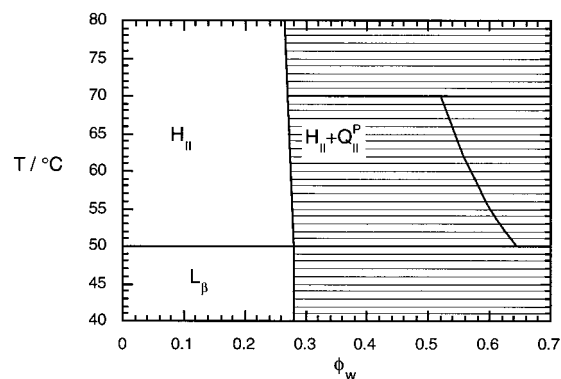


Figure 7. The phase diagram for 2:1 MA/DMPC at atmospheric pressure. There is some evidence of metastable bicontinuous phases of space group $Im3d$ and $Pn3m$ in the coexistence region $H_{II} + Q_{II}^P$.

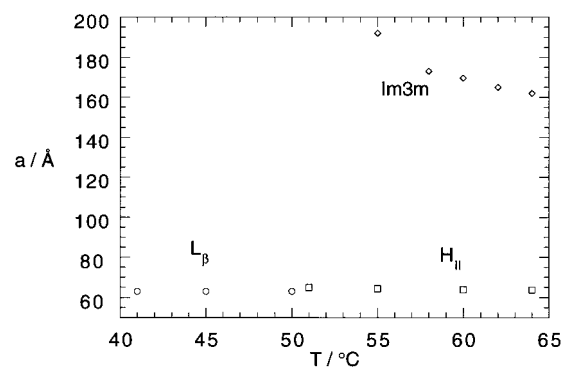


Figure 8. The lattice parameters of the excess water phases in 2:1 MA/DMPC.

ous X-ray evidence of both Q_{II}^G and Q_{II}^D . Because we find the H_{II} and Q_{II}^P phase in equilibrium in excess water, we must conclude that these are metastable phases and as such we have not included them in the phase diagram. Measurements of the lattice parameter of the $Im3m$ cubic phase, Figure 8, have been used to calculate the water composition of the phase, section 4.2. These measurements show that the bicontinuous cubic has a significantly greater water content than that observed in 2:1 LA/DLPC. In common with the 2:1 LA/DLPC system, the reproducibility of our measurements of the cubic lattice parameter are not as good as the H_{II} phase (for example the cubic lattice parameter measurement at 55 °C varied by $\pm 5\%$), which makes the phase boundary somewhat inaccurate. Even so it is quite clear that the cubic unit cell swells as we increase the chain length as does the H_{II} unit cell.

Our data are in good agreement with the neutron diffraction measurements of Seddon and co-workers.²⁵ The excess water phase boundary is in agreement with their measurements and the lattice parameters of the L_β and H_{II} phases are in good agreement (to within $\pm 2 \text{ Å}$). The cubic lattice parameters are in reasonable agreement with the neutron measurements being approximately 10 Å larger than reported here at 55 °C and 10 Å smaller at 65 °C . We do not find evidence in excess water of a $Pn3m$ cubic phase as reported by Heimburg and co-workers.²⁶

As one might anticipate from the trend in destabilizing the bicontinuous cubics with increasing chain length, any further increase leads to their complete disappearance.¹³

3.2. Molecular Geometry in 2:1 FA/PC Mixtures. We now go on to model the swelling behavior with water composition of the inverse bicontinuous and inverse hexagonal phases. This is both a necessary precursor to the energetic modeling of

these phases and an essential element in identifying the bicontinuous structure of the cubic phases.

As we have already stated, the pivotal surface is defined to be the location on the molecule whose area is invariant upon isothermal bending. This means that the mass of lipid either side of the pivotal surface must remain fixed as we bend the interface by reducing the water content of the system. Under this constraint and a geometrical model of the mesophase, this of course fixes the molecular geometry as a function of water composition. In the case of the H_{II} phase, we set the interfacial geometry to be cylindrical and then the relevant equation for relating lattice parameter to the water volume fraction is

$$a = \frac{2}{(1 - \phi_w)^{A_n/\nu}} \sqrt{\frac{2\pi}{\sqrt{3}} \left[1 - \frac{\nu_n}{\nu} (1 - \phi_w) \right]} \quad (2)$$

where A_n is the molecular area at the pivotal plane, ν_n is the molecular volume between this plane and the end of the chains, and ν is the total molecular volume. For the inverse bicontinuous cubics the interface is assumed to be parallel to the underlying minimal surface which give rise to the rather complex equation

$$a = \frac{\langle \nu \rangle}{\langle A_n \rangle (1 - \phi_w)} \left\{ -2\sigma_0 + \frac{2^{5/3} \sigma_0^2}{\sqrt[3]{4\sigma_0^3 + 9\pi\chi(1 - \phi_w)^2 \left(\frac{\langle \nu_n \rangle}{\langle \nu \rangle}\right)^2 + 3(1 - \phi_w) \left(\frac{\langle \nu_n \rangle}{\langle \nu \rangle}\right) \sqrt{\pi\chi(8\sigma_0^3 + 9\pi\chi(1 - \phi_w)^2 \left(\frac{\langle \nu_n \rangle}{\langle \nu \rangle}\right)^2)}}} + \frac{2^{1/3}}{\sqrt[3]{4\sigma_0^3 + 9\pi\chi(1 - \phi_w)^2 \left(\frac{\langle \nu_n \rangle}{\langle \nu \rangle}\right)^2 + 3(1 - \phi_w) \left(\frac{\langle \nu_n \rangle}{\langle \nu \rangle}\right) \sqrt{\pi\chi(8\sigma_0^3 + 9\pi\chi(1 - \phi_w)^2 \left(\frac{\langle \nu_n \rangle}{\langle \nu \rangle}\right)^2)}}} \right\} \quad (3)$$

where σ_0 is the dimensionless surface area of the minimal surface in the unit cell (3.0910 for G, 1.9189 for D, and 2.3451 for P), χ is the Euler characteristic in the unit cell (−8 for G, −2 for D, and −4 for P), and $\langle \dots \rangle$ indicates a surface average. The derivations of eqs 2 and 3 are given in the Appendix.

The pivotal surface geometry has been found by fitting our data of the lattice parameter as a function of the water volume fraction in the H_{II} phase and the bicontinuous cubic phases, Figure 9. We include an analysis of H_{II} data from C_{16} and C_{18} mixtures reported in ref 13. From density measurements made 10 °C above the chain melting transition we calculate the volume of the 2:1 FA/PC complexes to be 1735, 1941, 2144, and 2372 Å³ for C_{12} , C_{14} , C_{16} , and C_{18} mixtures, respectively. The values of ν recorded in Table 1 were obtained by applying a linear least-squares fit to these data (the fit indicates that each CH₂ group occupies a volume of 26.4 ± 0.2 Å³ which is in reasonable agreement with previous determinations). The area and volume of the pivotal surface for the 2:1 FA/PC complexes were found from least-squares fits to the swelling data of Figure 9.

It is interesting to note that the fit to the H_{II} data is far more constrained than that to the bicontinuous cubic data and this fit is what sets the small errors on our geometrical measurements. The model swelling curves for the inverse bicontinuous cubic and inverse hexagonal phases of the 2:1 LA/DLPC system use identical values of A_n and ν_n . The data from the H_{II} phases also appears to be more reproducible than for the inverse bicontinuous cubic phases. This may be because the H_{II} phase occurs at water contents which are below the excess water point of the gel phase. This means that if the L_β phase is homoge-

neously hydrated water does not need to be transported through the sample during heating. It is therefore rather straightforward to achieve good sample homogeneity in the H_{II} phase.

For the cubic phases, this is not the case. Here the water composition is greater than in the gel phase and considerable volumes of water may need to be transported through the parent mesophase. The reader may have noticed that data points for the three inverse bicontinuous cubic phases present in 2:1 LA/DLPC overlap in Figure 9b. This is because we have presented measurements collected over a 10° interval (35–45 °C) to use in our fit. We are able to do this, because at fixed water content the lattice parameter hardly varies at all with temperature (certainly less than the reproducibility of our results) and neither does the lipid's partial specific volume.

Of course the models we have used to fit our data assume that there are no defects in the mesophases which might sequester additional water or lipid. The consistency of the fits to our data, both across mesophases and samples is rather compelling evidence that, at least in these cases, the defect concentrations are probably rather low.

4. Discussion

4.1. Phase Behavior. The phase behavior we have observed in the 2:1 FA/PC mixtures has a number of apparently universal features.²⁷

As we increase the chain length of the homologous series we find that the inverse bicontinuous structures are destabilized and replaced by the inverse hexagonal phase. As we increase temperature or decrease the water content in systems containing the inverse bicontinuous cubics, we produce the same effect.

We will leave a detailed model-based discussion of the possible origin of this behavior until the second article in this series.¹ We can, however, make some general, qualitative observations, which give some sense of what is probably going on.

As we increase the chain length of our lipids one would anticipate that the longer the chains, the easier it would be to accommodate the variations in monolayer thickness that are required to pack the H_{II} phase.¹⁸ It is believed that packing frustration in the inverse bicontinuous cubic phases is negligible, so that this would reduce the free energy of the H_{II} phase relative to the cubics.^{28,29} It is normally assumed that increasing the chain length also increases the desire for negative mean curvature at the interface. If this is true then we would expect this to favor the H_{II} phase also, because the curvature inhomogeneities and their associated energetic cost in the inverse bicontinuous cubics should increase rapidly.²⁹ However, we should be cautious of making this assumption in the case of these systems. Both the water content and the lattice parameter of the H_{II} and the bicontinuous cubic phase in 2:1 MA/DMPC are greater than in the shorter chain length 2:1 LA/DLPC mixture. This inevitably means that the magnitude of the interfacial mean curvature in 2:1 MA/DMPC is less than in 2:1 LA/DLPC, and hence we would assume the desire for curvature is also less in 2:1 MA/DMPC. This contradicts our normal assumptions and will be examined in detail in the second article of this series.¹

If we increase the temperature the experimental evidence is however quite clear; the desire for interfacial mean curvature increases since both the cubic and H_{II} phases shrink in excess water. We might therefore explain the disappearance of the bicontinuous phases in terms of the increasing bending energy costs imparted by the ever increasing curvature inhomogeneity of the interface.²⁹ Decreasing the water content does not change

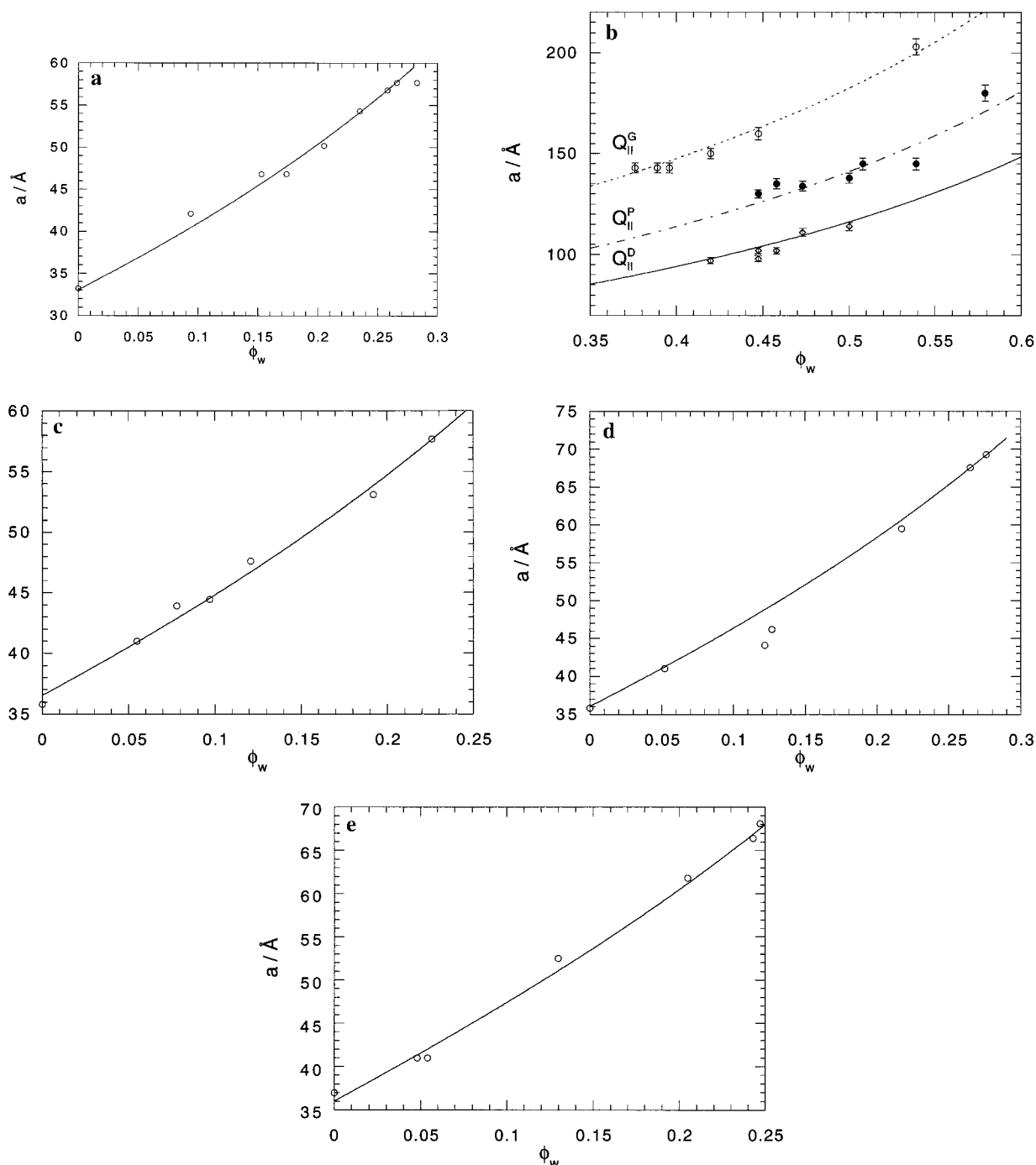


Figure 9. Theoretical fits to mesophase swelling data. (a) The H_{II} phase in 2:1 LA/DLPC at 40 °C. The least-squares fit to the data excludes the data points at $\phi_w = 0.094$ and 0.153 and the datum at 0.283 is included to indicate the excess water point. (b) The lattice parameters of the cubic phases in 2:1 LA/DLPC measured between 35 and 45 °C and the theoretical swelling laws. (c) The H_{II} phase in 2:1 MA/DMPC at 60 °C. (d) The H_{II} phase in 2:1 PA/DPPC at 70 °C. The least-squares fit to the data excludes the data points at $\phi_w = 0.122$ and 0.127. (e) The H_{II} phase in 2:1 SA/DSPC at 80 °C.

TABLE 1: Geometrical Parameters of the 2:1 FA/PC Mixtures

| chain length | $\nu/\text{\AA}^3$ | $\nu_n/\text{\AA}^3$ | $A_n/\text{\AA}^2$ | $(\nu - \nu_n)/\text{\AA}^3$ |
|-----------------|--------------------|----------------------|--------------------|------------------------------|
| C ₁₂ | 1736 ± 38 | 1230 ± 30 | 108 ± 2 | 506 ± 48 |
| C ₁₄ | 1948 ± 41 | 1334 ± 51 | 114 ± 3 | 614 ± 65 |
| C ₁₆ | 2160 ± 44 | 1677 ± 20 | 109 ± 1 | 483 ± 48 |
| C ₁₈ | 2372 ± 47 | 1899 ± 30 | 112 ± 2 | 473 ± 56 |

the desire for curvature, as long as the polar groups remain fully hydrated, but geometrically limits it. Nevertheless, this means that the curvature elastic energy cost bound up in the curvature inhomogeneity of the bicontinuous cubics will eventually

destabilize these phases. At extremely negative mean interfacial curvatures the difficulty of packing chains in the hexagonal phase will of course also be relaxed.¹⁸

There are a number of other apparently generic aspects to the phase behavior which one cannot explain using qualitative arguments.

The ordering of the inverse bicontinuous cubic phases with increasing water content follows the pattern $Q_{II}^G \rightarrow Q_{II}^D \rightarrow Q_{II}^P$. This appears to be universal,³⁰ although either end of the sequence may not appear in a particular system. The pattern is set by the space filling properties of the underlying minimal surfaces, but current energetic models^{29,31} predict that the energy

of these phases should be degenerate. The experimental evidence we have collected indicates that this is not the case.

As we increase temperature we observe a phase transition $Q_{II}^P \rightarrow Q_{II}^D$. Again current theories cannot model such a transition. We will show, in the second of this series of reports,¹ that it is possible to explain this transition and the phase ordering with water composition if the interface is not constrained to remain parallel to the underlying minimal surface.

4.2. Mesophase Geometry. Recently there has been some debate regarding the authenticity of the identification of the *Im3m* cubic phase with a bicontinuous structure based on the P minimal surface.³² Our X-ray structural measurements provide evidence that, at least in this case, all three cubic phases are inverse bicontinuous structures based on the G, D, and P minimal surfaces.

First there is the evidence of a fixed ratio in the lattice parameters of coexisting cubics of spacegroup *Im3m* and *Pn3m*, which is in agreement with theoretical predictions for the P and D surface cubics. Investigations of 2:1 FA/PC systems under hydrostatic pressure³³ confirms the existence of this fixed ratio over a wide range of thermodynamic conditions.

Second there is the evidence which shows that the lattice parameter measurements of the bicontinuous cubics concur with the theoretical swelling law. Given that the swelling law is based on the differential geometric properties of the underlying minimal surface, this is strong evidence that the three cubic structures are the bicontinuous cubics Q_{II}^G , Q_{II}^D , and Q_{II}^P .

4.3. Molecular Geometry and Intermolecular Forces. Within the precision of our measurements, the position and cross-sectional area of the pivotal surface is constant over the entire range of water composition in each of our 2:1 FA/PC systems. In the case of 2:1 LA/DLPC, this is true within all four inverse mesophases. Indeed as far as we are aware a self-consistent fit of swelling data over such a wide range (from $\phi_w = 0.00$ to 0.58) and covering four distinct mesophases has never previously been recorded. Furthermore the location and area of the pivotal surface changes very little as we increase chain length. We have found linear relationships between A_n and ν_n and the number of carbon atoms per hydrophobic chain n_c ,

$$A_n = (100.5 \pm 5) + (0.6 \pm 0.3)n_c \quad (4)$$

and

$$\nu_n = (-108 \pm 3) + (111.5 \pm 0.2)n_c \quad (5)$$

We have omitted the C_{14} data points from these fits because they appear to be systematically displaced from the straight line. (This is not the case for our densitometric measurements of ν , implying that is a systematic error in our hydration sequence data for the C_{14} system.) The data indicates a trend toward an increase in the area of the pivotal surface with increasing chain length and the gradual movement of the pivotal surface toward the headgroup at a rate of 0.05 Å per additional carbon atom. These changes are not dramatic, so it is worthwhile noting that the weighted mean of $A_n = 109.5 \pm 1.5$ Å² and the weighted mean of $\nu - \nu_n = 508 \pm 42$ Å³, where the weighting is given by the quoted error for each measurement. These values place the pivotal surface for every system between the second and third CH₂ group of the phosphatidylcholine molecule.

These measurements show that the geometrical behavior of these 2:1 FA/PC mixtures during interfacial bending is very simple. It is therefore appropriate to ask why this may be. In previous measurements of the swelling behavior of lyotropic mesophases it has been observed that as one reduces the water

composition the location of the pivotal surface moves (normally toward the polar/apolar interface).³⁴ It has been inferred that this is due to the headgroups being forced into such close proximity by the increasing interfacial curvature, that steric headgroup–headgroup interactions become strongly repulsive. It has been suggested previously from theoretical calculations that the pivotal surface should be located near the most incompressible part of the amphiphiles hydrocarbon chain and this is located around the second or third carbon for a saturated hydrocarbon chain.¹¹ This would, however, only be so if any repulsive interactions in the headgroup region were relatively small. So all of our measurements indicate that there is little or no headgroup–headgroup resistance to bending in saturated 2:1 FA/PC mixtures.

In this regard it is interesting to estimate how the sum of the molecular cross sectional areas for two fatty acids and one phosphatidylcholine compares to the pivotal surface cross section we have found. We do this for 2:1 LA/DLPC. We have measured the cross sectional area of DLPC in the L_α phase at 25 °C (R. H. Templer, unpublished results) using Luzzati's approach³⁵ and obtain 63 ± 1 Å². We have estimated the cross-sectional area of LA from the value of the molecular volume of LA in the fluid state (370 Å³)³⁶ and the assumption that the LA lies between the glycerol backbone of the DLPC molecules and the terminal CH₃ group. This gives a cross-sectional area for LA of 26 Å². Summing the individual components for a 2:1 LA/DLPC complex we obtain 115 Å². This is 7 Å² greater than the area calculated for the pivotal surface. If our estimate is correct, then this might lend support to the idea that there is direct hydrogen bonding between the carboxylic acid and phosphate moieties,¹² with the fatty acid headgroups lying close to the glycerol backbone of the phosphatidylcholine molecule. Notwithstanding this possibility, it is clear that the cross-sectional area around the phosphatidylcholine headgroup, provided by being complexed with two fatty acids, is greater than is required for full headgroup hydration of the phosphatidylcholine on its own. At the same time the lateral pressure in the chain region must have increased since the average area per chain has decreased upon adding fatty acid. This then drives the interface to bend. The excess cross-sectional area around the phosphatidylcholine headgroup region means that the interface can maintain high degrees of monolayer curvature before they begin to experience strong steric repulsions from their neighbors. Our measurements and these observations are consistent with theoretical predictions of the behavior of the pivotal plane where headgroup interactions are "soft".³⁷

Acknowledgment. This work was funded in part by the EPSRC (Grant GR/K21054), the Royal Society, and a British Council-DAAD grant. N.A. Warrender wishes to acknowledge the financial assistance of the Harwell Laboratory of the UKAEA and Z. Huang acknowledges the financial support of the K.C. Wong Fellowship.

Appendix

The H_{II} Phase. To derive the relationships relating the lattice parameter to the water volume fraction one must first define the geometry of the pivotal plane. In the case of the H_{II} phase we will assume that it is cylindrical. From our operational definition of the pivotal surface we can set a simple geometrical constraint on the system, which is that over the unit cell, the area at the pivotal surface divided by the lipid volume between it and the unit cell boundaries should be constant with hydration. This ratio will of course be equal to A_n/ν_n . After some simple

geometry, the application of this constraint gives us

$$R_n = \sqrt{\left(\frac{\nu_n}{A_n}\right)^2 + \frac{\sqrt{3}}{2\pi}a^2} - \frac{\nu_n}{A_n} \quad (\text{A1})$$

where R_n is the radial distance from the center of the water channel to the pivotal surface.

We find a by noting that the pivotal surface volume fraction $(1 - \phi_w)\nu_n/\nu$ is equal to $1 - 2\pi R_n^2/\sqrt{3}a^2$. Solving for a we find the required relationship

$$a = \frac{2}{(1 - \phi_w)^{A_n/\nu}} \sqrt{\frac{2\pi}{\sqrt{3}} \left[1 - \frac{\nu_n}{\nu} (1 - \phi_w) \right]} \quad (\text{A2})$$

Inverse Bicontinuous Cubic Phases. In the case of the inverse bicontinuous cubic phases, we assume that the pivotal plane is parallel to the underlying periodic minimal surface.²⁰ From differential geometry¹⁰ we know that the area of a parallel patch, $A(z)$, projected away from the minimal surface by a distance z is related to the area of the original patch A_0 by

$$A(z) = A(0)(1 + Kz^2) \quad (\text{A3})$$

where K is the Gaussian curvature (given by the product of c_1 and c_1) in the locality of the original patch. The volume swept out in this projection $\nu(z)$, is given by

$$\nu(z) = A(0)z \left(1 + \frac{1}{3}Kz^2 \right) \quad (\text{A4})$$

We can use eqs A3 and A4 to find A_n , ν_n , or ν in terms of K and the distance from the minimal surface to the pivotal surface ξ , and in the case of ν , from the minimal surface to the polar/apolar interface l . However, because the curvature of the underlying minimal surface is inhomogeneous we must calculate surface averaged values of A_n , ν_n , and ν . In fact, for our purposes it suffices to calculate the ratio A_n/ν_n .

$$\frac{\langle A_n \rangle}{\langle \nu_n \rangle} = \frac{1}{\xi} \left(\frac{1 + \langle K \rangle \xi^2}{1 + \frac{1}{3} \langle K \rangle \xi^2} \right) \quad (\text{A5})$$

Using the Gauss–Bonnet theorem one can relate $\langle K \rangle$ to the lattice parameter via

$$\langle K \rangle = \frac{2\pi\chi}{\sigma_0 a^2} \quad (\text{A6})$$

where χ is the Euler characteristic of the minimal surface in the unit cell and σ_0 is the dimensionless area of the minimal surface, also in the unit cell. Values for the G, D, and P surfaces are quoted in the main text.

With eqs A5 and A6, we can find an expression for the lattice parameter as a function of the distance to the pivotal surface from the underlying minimal surface. It therefore remains only to determine how ξ varies with ϕ_w in order to obtain the expression we require. We do this by noting that the volume fraction in the unit cell between the pivotal surface and minimal surface, $\langle \nu_n \rangle / \langle \nu \rangle (1 - \phi_w)$ is related to ξ by³⁸

$$\frac{\langle \nu_n \rangle}{\langle \nu \rangle} (1 - \phi_w) = 2\sigma_0 \left(\frac{\xi}{a} \right) + \frac{4}{3} \pi \chi \left(\frac{\xi}{a} \right)^3 \quad (\text{A7})$$

Combining eqs A5, A6, and A7 we obtain a cubic equation in a ,

$$\left(\frac{A_n}{\nu} \right)^3 a^3 + 6\sigma_0 \left(\frac{A_n}{\nu} \right)^2 \frac{a^2}{(1 - \phi_w)} - \left[\frac{36\pi\chi}{(1 - \phi_w)} \left(\frac{\nu_n}{\nu} \right)^2 + \frac{32\sigma_0^3}{(1 - \phi_w)^3} \right] = 0 \quad (\text{A8})$$

which when solved gives

$$a = \frac{\langle \nu \rangle}{\langle A_n \rangle (1 - \phi_w)} \left\{ -2\sigma_0 + \frac{2^{5/3} \sigma_0^2}{\sqrt[3]{4\sigma_0^3 + 9\pi\chi(1 - \phi_w)^2 \left(\frac{\langle \nu_n \rangle}{\langle \nu \rangle} \right)^2 + 3(1 - \phi_w) \left(\frac{\langle \nu_n \rangle}{\langle \nu \rangle} \right) \sqrt{\pi\chi \left(8\sigma_0^3 + 9\pi\chi(1 - \phi_w)^2 \left(\frac{\langle \nu_n \rangle}{\langle \nu \rangle} \right)^2} \right)}} + \frac{2^{1/3}}{\sqrt[3]{4\sigma_0^3 + 9\pi\chi(1 - \phi_w)^2 \left(\frac{\langle \nu_n \rangle}{\langle \nu \rangle} \right)^2 + 3(1 - \phi_w) \left(\frac{\langle \nu_n \rangle}{\langle \nu \rangle} \right) \sqrt{\pi\chi \left(8\sigma_0^3 + 9\pi\chi(1 - \phi_w)^2 \left(\frac{\langle \nu_n \rangle}{\langle \nu \rangle} \right)^2} \right)}} \right\} \quad (\text{A9})$$

References and Notes

- (1) Templer, R. H.; Seddon, J. M.; Duesing, P. M.; Winter, R.; Erbes, J. *J. Phys. Chem.* **1998**. In press.
- (2) Landh, T. *FEBS Lett.* **1995**, 369, 13.
- (3) Lindblom, G.; Rilfors, L. *Biochim. Biophys. Acta* **1989**, 988, 221.
- (4) Ellens, H.; Siegel, D. P.; Alford, D.; Yeagle, P. L.; Boni, L.; Lis, L. J.; Quinn, P. J.; Bentz, J. *Biochemistry* **1989**, 28, 3692.
- (5) Schramm, M. *Biochim. Biophys. Acta* **1967**, 135, 44.
- (6) Kantor, H. L.; Prestegard, J. H. *Biochemistry* **1978**, 17, 3592.
- (7) Ordway, R. W.; Singer, J. J.; Walsh, J. V. *Trends Neurosci.* **1991**, 14, 96.
- (8) Gruner, S. M. *Proc. Natl. Acad. Sci. U.S.A.* **1985**, 82, 3665.
- (9) Andersson, S.; Hyde, S. T.; Larsson, K.; Lidin, S. *Chem. Rev.* **1988**, 88, 221.
- (10) Hyde, S. T. *J. Phys. Chem.* **1989**, 93, 1458.
- (11) Szleifer, I.; Kramer, D.; Ben-Shaul, A.; Gelbart, W. M.; Safran, S. A. *J. Chem. Phys.* **1990**, 92, 6800.
- (12) Boggs, J. M. *Biochim. Biophys. Acta* **1987**, 906, 353.
- (13) Seddon, J. M.; Templer, R. H.; Warrender, N. A.; Huang, Z.; Cevc, G.; Marsh, D. *Biochim. Biophys. Acta* **1997**, 1327, 131.
- (14) Koynova, R.; Tenchov, B.; Rapp, G. *Chem. Phys. Lipids* **1997**, 88, 45.
- (15) Janiak, M. J.; Small, D. M.; Shipley, G. G. *J. Biol. Chem.* **1984**, 23, 1093.
- (16) Luzzati, V.; Vargas, R.; Gulik, A.; Mariani, P.; Seddon, J. M.; Rivas, E. *Biochemistry* **1992**, 31, 279.
- (17) Kirk, G. L.; Gruner, S. M.; Stein, D. E. *Biochemistry* **1984**, 23, 1093.
- (18) Duesing, P. M.; Templer, R. H.; Seddon, J. M. *Langmuir* **1997**, 13, 351.
- (19) Templer, R. H.; Warrender, N. A.; Seddon, J. M. *Biophys. Chem.* **1994**, 49, 1.
- (20) Templer, R. H. *Langmuir* **1995**, 11, 334.
- (21) For example, see: Kozlov, M.; Leikin, S.; Rand, R. P. *Biophys. J.* **1994**, 66, 299.
- (22) Templer, R. H.; Gruner, S. M.; Eikenberry, E. F. *Adv. Electron Phys.* **1988**, 24, 275.
- (23) Warrender, N. A. Ph.D. Thesis, Imperial College, 1992.
- (24) Anderson, D. M.; Davis, H. T.; Scriven, L. E.; Nitsche, J. C. C. *Adv. Chem. Phys.* **1990**, 77, 337.
- (25) Seddon, J. M.; Hogan, J. L.; Warrender, N. A.; Pebay-Peroula, E. *Prog. Colloid Polym. Sci.* **1990**, 81, 189.
- (26) Heimburg, T.; Ryba, N.; Wurz, U.; Marsh, D. *Biochim. Biophys. Acta* **1990**, 1025, 77.
- (27) Seddon, J. M.; Templer, R. H. *Philos. Trans. R. Soc. London A* **1993**, 344, 377 and references therein.
- (28) Anderson, D. M.; Gruner, S. M.; Leibler, S. *Proc. Natl. Acad. Sci. U.S.A.* **1988**, 85, 5364.
- (29) Templer, R. H.; Turner, D. C.; Harper, P.; Seddon, J. M. *J. Phys. II France* **1995**, 5, 1053.
- (30) For example, see: e.g. Hyde, S. T.; Andersson, S.; Ericsson, B.; Larsson, K. Z. *Krystallogr.* **1984**, 168, 213. Turner, D. C.; Wang, Z.-G.; Gruner, S. M.; Mannock, D. A.; McElhaney, R. N. *J. Phys. II France* **1992**, 2, 2039. Briggs, J.; Chung, H.; Caffrey, M. *J. Phys. II France* **1995**, 5, 1649.
- (31) Helfrich, W.; Rennschuh, H. *J. Phys. Paris* **1990**, 51, (C7)189.
- (32) Luzzati, V. *J. Phys. II France* **1995**, 5, 1649.

- (33) Erbes, J. Ph.D. Thesis, Dortmund University, 1996.
- (34) Rand, P. R.; Fuller, N.; Gruner, S. M.; Parsegian, A. V. *Biochemistry* **1990**, 29, 76.
- (35) Luzzati, V. In *Biological Membranes*; Chapman, D., Ed.; Academic Press: London, 1968; Vol. 1, p 71.
- (36) Small, D. M. In *Handbook of Lipid Research*; Hanahan, D. J., Ed.; Plenum Press: New York, 1988; Vol. 4, p 233.
- (37) Ennis, J. *J. Chem. Phys.* **1992**, 97, 663.
- (38) Turner, D. C.; Wang, Z.-G.; Gruner, S. M.; Mannock, D. A.; McElhaney, R. N. *J. Phys. II France* **1992**, 2, 2039.